ACS OMEGA

Article

http://pubs.acs.org/journal/acsodf

Graphene Oxide-Coated Surface: Inhibition of Bacterial Biofilm Formation due to Specific Surface−Interface Interactions

Nisha Yadav,[†] Amrita Dubey,[‡] Swapnil Shukla,[†] Chetan Prakash Saini,[§] Govind Gupta,[∥] Richa Priyadarshini,*[,‡] and Bimlesh Lochab*[,†]

[†]Department of Chemistry, [‡]Department of Life Sciences, and [§]Department of Physics, School of Natural Sciences, Shiv Nadar University, Gautam Buddha Nagar, Uttar Pradesh 201314, India

[∥]Physics of Energy Harvesting, TEC Building, CSIR-National Physical Laboratory, Dr. K.S. Krishnan Marg, New Delhi 110012, India

Supporting Information

ABSTRACT: Graphene oxide (GO) is a promising and remarkable nanomaterial that exhibits antimicrobial activity due to its specific surface−interface interactions. In the present work, for the first time, we have reported the antibacterial activity of GO-coated surfaces prepared by two different methods (Hummers' and improved, i.e., GO_H and GO_I) against bacterial biofilm formation. The bacterial toxicity of the deposited GO-coated surfaces was investigated for both Gram-negative (*Escherichia coli*) and Gram-positive (*Staphylococcus aureus*) models of bacteria. The mechanism of inhibition is different on the coated surface than that in suspension, as determined by measurement of the percentage inhibition of biofilm formation, Ellman's assay, and colony forming unit (CFU) studies. The difference in the nature, degree of oxidative functionalities, and size of the synthesized GO nanoparticles mitigates biofilm formation. To better understand the antimicrobial mechanism of GO when coated on surfaces, we were able to demonstrate that beside reactive oxygen species-mediated oxidative stress, the physical properties of the GO-coated substrate effectively inactivate bacterial cell proliferation, which forms biofilms. Light and atomic force microscopy (AFM) images display a higher inhibition in the proliferation of planktonic cells in Gram-negative bacteria as compared to that in Gram-positive bacteria. The existence of a smooth surface with fewer porous domains in GO_I inhibits biofilm formation, as demonstrated by optical microscopy and AFM images. The oxidative stress was found to be lower in the coated surface as compared to that in the suspensions as the latter enables exposure of both a large fraction of the active edges and functionalities of the GO sheets. In suspension, GO_H is selective against *S. aureus* whereas GO_I showed inhibition toward *E. coli*. This study provides new insights to better understand the bactericidal activity of GO-coated surfaces and contributes to the design of graphene-based antimicrobial surface coatings, which will be valuable in biomedical applications.

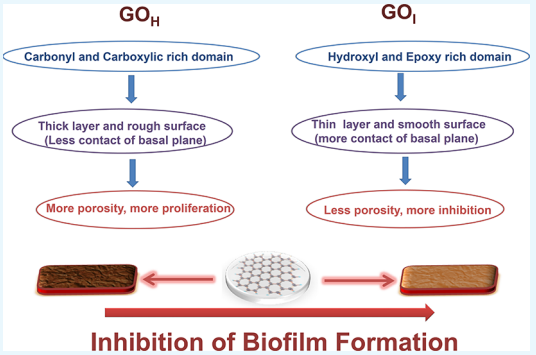

1. INTRODUCTION

Graphene is a two-dimensional single-atom-thick sheet of sp^2-hybridized carbon atoms arranged in a hexagonal array.[1] The attractive electronic, thermal, and mechanical properties of graphene have generated exceptional interest in the research community and its utilization in applications ranging from electro-optic to biomedical devices has been studied.[2] Most of the practical applications, especially at industry level, demand a cost-effective, scalable preparation of graphene with easy processability whilst retaining its beneficial properties, and this is most efficiently resolved by its graphene oxide (GO) derivative. GO is produced in a facile manner from a naturally occurring allotrope of carbon, graphite. GO possesses oxidative functionalities, such as phenolic hydroxyl, carbonyl, epoxide, and carboxylic groups, that enables their good water dispersibility.[3] GO can either be utilized as produced, it can undergo reduction to form reduced GO (rGO), or it can be further chemically modified to widen its scope of applications. The presence of oxidative functionalities has imparted GO with an inherent toxicity that impedes its application in the medical field. The adverse effects shown by GO include the generation of reactive oxygen species (ROS), DNA damage, cell apoptosis, inflammatory cell infiltration, pulmonary edema, etc.[4] The issue of toxicity is generally handled by coupling the oxidative functionalities with biocompatible polymers to advance their applications as nanocarriers for drug delivery to cell imaging.[5−7] However, the presence of such oxidative functionalities can be taken as an advantage to circumvent problems where cell death is desired. A major health problem is bacteria-induced infectious diseases that affect millions of people worldwide annually. To safeguard public health and quality of life, several products have been designed with antibacterial materials to prevent or restrict bacterial growth during their usage. Such infections are widely treated or inhibited using antibiotic

Received: March 29, 2017
Accepted: June 14, 2017
Published: July 3, 2017

DOI: 10.1021/acsomega.7b00371
ACS Omega 2017, 2, 3070−3082

drugs,[8] which are ineffective due to the simultaneous development of resistance against many strains.[9] Research on novel materials such as metal nanoparticles[10,11] and ammonium compounds[12] is still ongoing to prevent such proliferation of bacterial diseases. All of these compounds, especially antibiotic drugs, involve multistep syntheses which are both time-consuming and cost ineffective, and may display lower efficacies after their tedious and lengthy synthetic protocols. In addition, the associated environmental issues of their large-scale production cannot be ignored. Therefore, alternative simplistic methodologies need to be found to provide commercially viable solutions to inhibit such bacterial proliferation.

Previous studies on carbon nanomaterials, such as carbon nanotubes, fullerene, and graphene, have shown appreciable and promising antimicrobial activities.[13−15] The cytotoxic effect of these materials was found to be dependent on both the nature of the nanomaterial and the type of bacteria. Understanding the nanomaterial perspective, size, degree and nature of oxidation,[15] and electronic state[16] may be the key to dictating its antimicrobial properties. These parameters can be controlled synthetically, accounting for the importance of the quantum confinement effect and miniaturization, as a forward strategy for identifying and designing novel antimicrobial materials. Amongst all the nanomaterials, graphene materials have gained importance due to their relatively larger sheet size and higher specific surface areas enabling higher efficacies. In addition, the combination of simpler synthetic protocols, the coexistence of hydrophilic (due to oxidative functionalities) and hydrophobic graphitic domains, along with nanoscale thickness provides great promise for their use in a wider set of applications including antimicrobial activity. Most publications have focused on the antibacterial activity of GO nanomaterials toward Gram-negative bacteria, *Escherichia coli*, and percentage inhibition was determined on their suspensions by colony forming unit (CFU) measurement.[17−19] The stability of the suspended GO nanoparticles in the dispersions within the incubation time with the bacteria is of paramount importance as it may dictate the percentage inhibition and mechanisms involved in killing the bacterial cells. The cell growth inhibition mechanisms of the graphene materials may be mediated via physical or chemical means leading to reversible and irreversible bacteriostatic and bactericidal effects, respectively. The mechanisms proposed to explain the inhibitory effect of GO-suspended nanoparticles include the direct contact mechanism,[17] oxidative stress,[18] and the wrapping/trapping of bacteria[19] in aggregated nanosheets leading to cell suffocation and thereby prevention of their proliferation. The chemical reason is attributed to the over-production of ROS that disintegrate the cell membrane, followed by cell death via production of lipid peroxides.[20] The antimicrobial properties of GO involving the cellular aggregation, wrapping, and piercing of the cell membrane were found to be dependent on sheet size and the presence of sharp edges. For example, Liu et al. reported that the lateral dimension of the GO sheet increases from 0.01 to 0.127 μm^2 leading to an increase in the loss of cell viability due to poor cell proliferation in GO-wrapped cells.[21] A similar result was reported wherein an increase in sheet area size of GO from 0.01 to 0.65 μm^2 led to an enhancement in antimicrobial effect due to cell entrapment by the larger sheet size.[18] It was observed that the reduced form of GO and its precursor, rGO and graphite, respectively, showed higher antibacterial activity than that of their oxidized forms due to their different electronic properties beside their larger particle size.[19] Conductive graphitic materials, such as rGO and graphite, have shown higher oxidation capacities than those of insulating GO materials because of the formation of a conductive bridge over the insulating lipid bilayer of a cell due to oxidative stress. The destructive extraction of lipid molecules may happen due to the interaction of the lipophilic nature of graphene-rich materials.[22]

The antimicrobial activity of GO has been explored mainly as an aqueous dispersion against the population growth of bacteria. In comparison to suspension assays, the antimicrobial effect of graphene as a film has also been studied but not to such a great extent. Reduced graphene and GO paper as free standing and flexible paper prepared via vacuum filtration have shown effective inhibition against *E. coli*. GO films were shown to have a relatively higher inhibition activity than that of rGO, which was attributed to the presence of different surface charges and functional groups.[23] Akhavan et al. discussed the antibacterial effect of electrophoretic-deposited nanosheets of a GO−magnesium salt nanocomposite on a stainless steel substrate.[13] Perreault et al. demonstrated that a GO-coated cellulosic filter causes bacterial inactivation due to direct contact between the bacterial cell and the GO-coated surface. The number of live *E. coli* cells decreases with decreasing GO sheet size.[18] Recently, Zhou et al. demonstrated that the existence of a wrinkled surface in GO films has a profound effect on the antibacterial properties.[24] A correlation was shown of the surface roughness of the corrugated surface with the size of the bacterial cell to demonstrate the antibacterial activity.

The GO nanomaterial reported in most antibacterial studies involves GO preparation using the modified Hummers and Offeman's method. The studies so far have included variation of either the size of the nanosheet or functionality via reduction to rGO and the analysis has mainly been based on bacterial suspensions using colony count or turbidometry methods. There have been no reports until now on the exploration of other synthetic methodologies of GO preparation via other routes and their effectiveness against bacterial biofilm formation.

Most bacteria in the environment exist as surface-associated, sessile bacterial communities, known as biofilms.[25] Biofilms are enclosed in an exopolysaccharide matrix, which shields the bacteria from the outside environment making it harder for antibiotics to penetrate and kill bacterial cells.[26] Hence, in a clinical setting, the development of biofilms leads to severe complications and re-infections, including cystic fibrosis, chronic otitis media, and urinary tract infections. For example, *Staphylococcus aureus*, a Gram-positive cocci, is the causative agent of a variety of diseases ranging from minor skin infections to endocarditis and toxic shock syndrome. *S. aureus* is also capable of biofilm formation, which increases its persistence and boosts its levels of antimicrobial resistance. Biofilms of *S. aureus* have been observed on catheters, pacemakers, and medical implants. Moreover, with the emergence of antibiotic-resistant *S. aureus* strains, such as the methicillin-resistant *S. aureus* (MRSA), these infections have caused increased morbidity and mortality.[27] Reoccurring urinary tract infections have been attributed to biofilm formation by uropathogenic *E. coli* (UPEC).[28,29] The treatment of biofilm-mediated infections is a big challenge that demands more sensitive and effective anti-biofilm strategies for their removal or reduction.

In recent years, the use of graphene and GO and their applications in antibacterial materials have been reported.[18,19,21] The importance of graphene coated on a substrate, with a

DOI: 10.1021/acsomega.7b00371
ACS Omega 2017, 2, 3070−3082

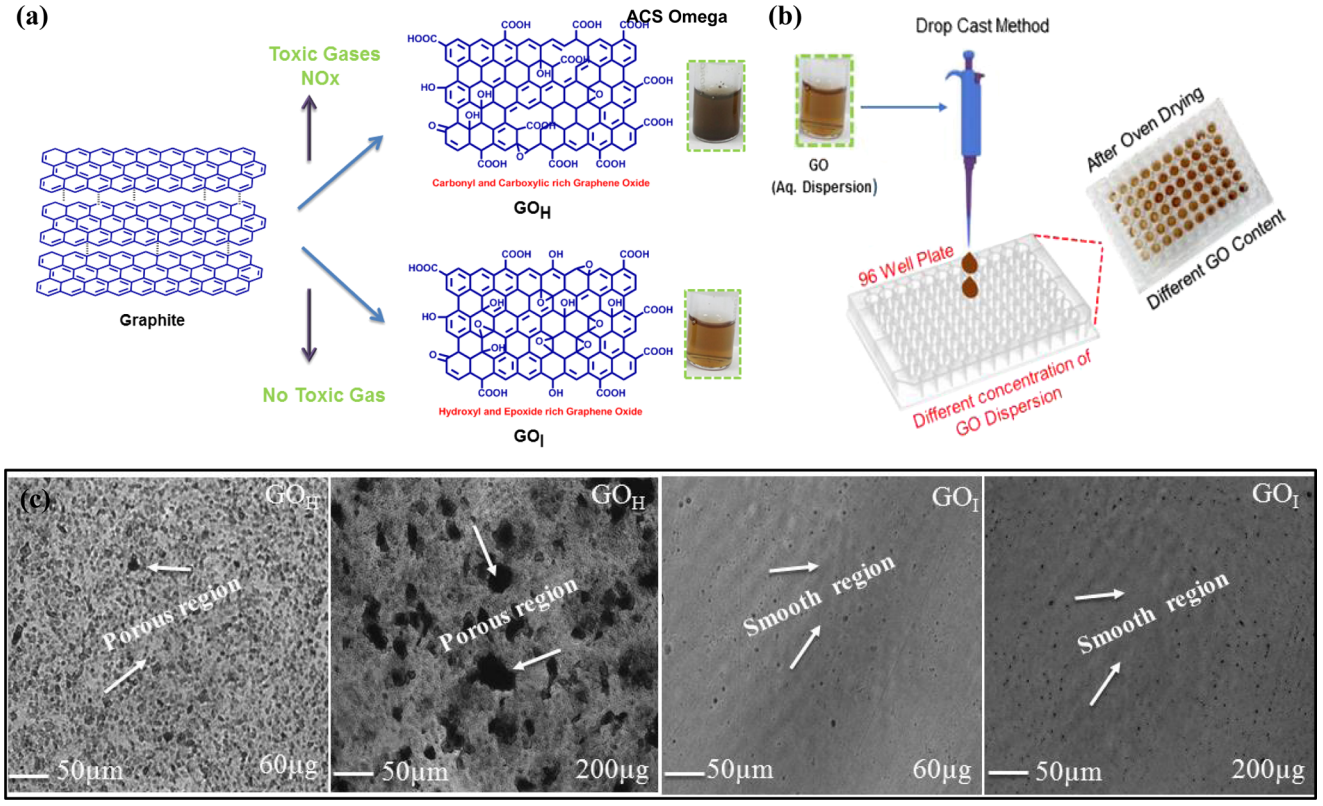

Figure 1. Overview of the synthetic methodology for the preparation of GO and the fabrication process. (a) Left: Schematic showing the preparation of GO via the Hummers' method and improved method. Inset shows the respective dispersions of GO at the same concentration (0.5 mg/mL). (b) Right: Drop-casting method of the GO aqueous dispersion onto a 96-well plate followed by slow air-oven drying to allow evaporation of water to form the GO-coated surface on the well plate. (c) Representative light microscopy images of the drop-casted GO-coated surface (GO_H and GO_I) at different solid contents. The black regions are the porous domains formed in the coated GO surface, and the gray area represents the GO nanosheets. At higher solid contents, the porosity of the GO_H coating is much higher. The GO_I surface showed a comparatively less porous surface. Scale bar = 50 μm.

particular emphasis on the potential of anti-biofilm formation, has been described by Parra et al.[30,31] The nature of graphene and bacteria surfaces is of paramount importance in dictating surface energy, wettability, and electrostatic interactions, which is essential for bacterial adhesion and to induce anti-biofouling properties. Dellieu et al.[32] demonstrated that the conductivity of a graphene film on a gold substrate has no role in the antibacterial properties. Further, Li et al. suggested that the antibacterial properties of graphene proceed via a charge transfer mechanism.[33] However, the mechanism of the interactions of GO coated on a substrate has not been reported and needs further exploration as it is currently not well understood. Further, applications exploiting the antibacterial effects of graphene for water purification, polymeric films for biomedical devices, antimicrobial fabric materials, and biofilm-resistant surfaces require its usage as a membrane rather than as a suspension. Therefore, to mimic a similar environment to that required in the above-mentioned applications, studies on GO-coated surface need to be performed. This has motivated us to explore the antibacterial effect of GO synthesized via two different routes and also the effect of these materials against bacterial biofilm formation. The present work involves the potential of GO synthesized from the traditional Hummers' method and an improved method, differing in the functionality and size of the GO produced, its characterization, and the effect on antibacterial behavior after immobilization on the surface. The bacterial strains utilized were pathogenic and non-pathogenic, *S. aureus* and *E. coli*, respectively, and are known to form biofilms. In addition, to understand the difference in antimicrobial activity, GO coated on the substrate and as an aqueous dispersion were also studied.

2. RESULTS AND DISCUSSION

2.1. Preparation and Characterization of GO Nanosheets and Their Deposition. In the present study, GO was synthesized by oxidizing natural graphite using the traditional Hummers' method (GO_H) and an improved method (GO_I) (Figure 1a). The Hummers' method is the most commonly used synthetic protocol, and involves graphite being chemically exfoliated by treatment with $KMnO_4$ and $NaNO_3$ in concentrated H_2SO_4.[34] This procedure is hazardous, especially during scale up, as it involves the generation of the toxic gas(es) NO_x in large volumes. In the improved method, the reaction eliminates the usage of $NaNO_3$, which consequently eliminates toxic gas evolution simultaneously maintaining good yields, making it a versatile strategy for the large-scale production of GO.[35] The aqueous dispersion of GO prepared by the two different methods is shown in Figure 1a. Previous reports on antibacterial activity have mainly been based on GO synthesized by the modified Hummers and Offeman's method. The equivalent of $KMnO_4$ used in the traditional Hummers' method is half that used in the modified Hummers and Offeman's method. The GO (GO_H and GO_I) nanoparticles synthesized in the current work differ significantly both

DOI: 10.1021/acsomega.7b00371
ACS Omega 2017, 2, 3070−3082

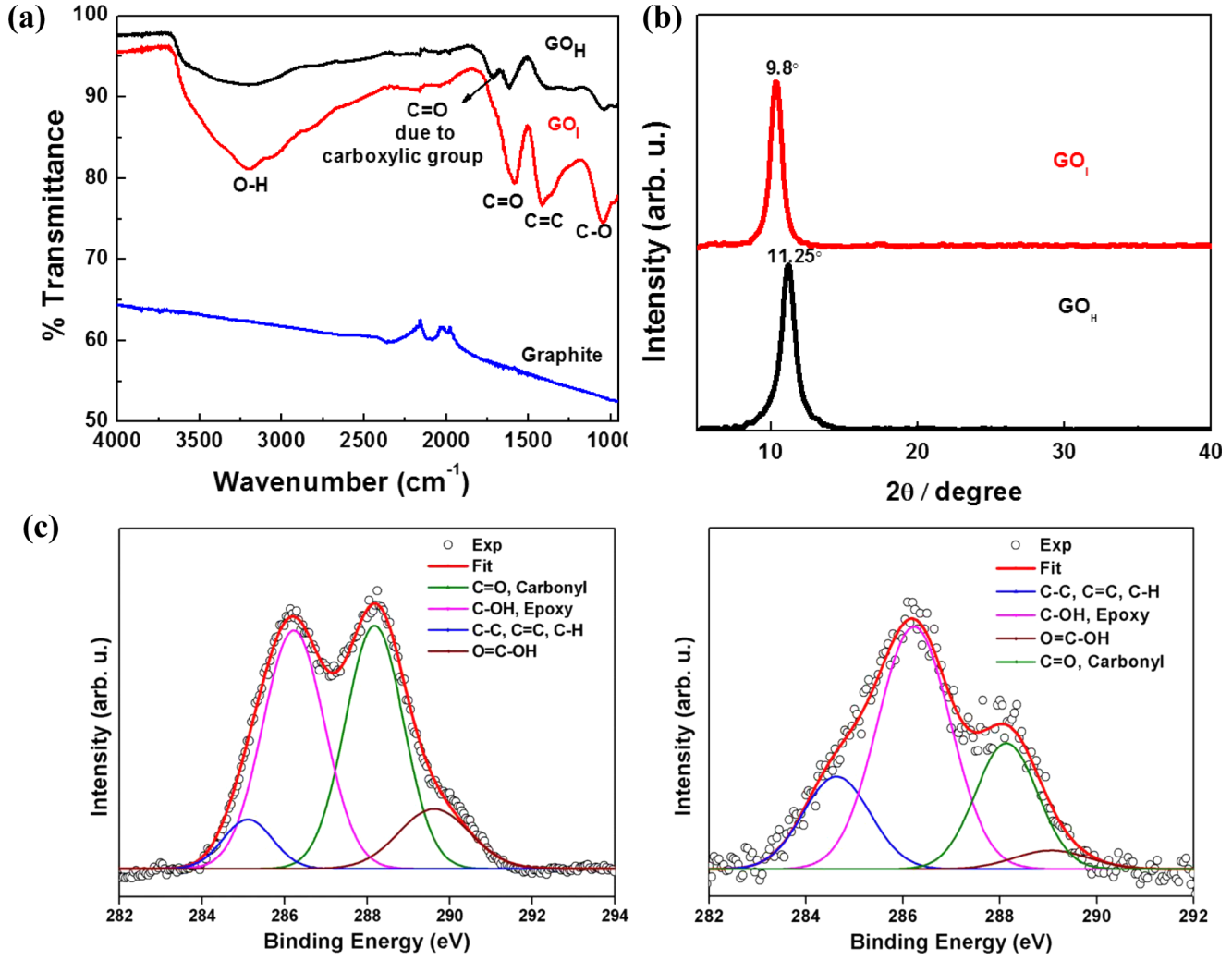

Figure 2. (a) FT-IR spectra, (b) XRD patterns, and (c) high-resolution deconvoluted C 1s XPS spectra of GO_H and GO_I.

chemically and physically in terms of degree of functionality and size as compared to that of GO described in other reports on its antibacterial properties. The variation in color of the dispersions, at the same concentration of nanoparticles, prepared by the Hummers' and improved method is suggestive of the different physiochemical properties of the two GO samples (as shown in the inset of Figure 1a).

Figure 1b shows the schematic of the fabrication process utilized to prepare the GO coated onto the 96-well plate. Pristine GO films are known to form self-assembled controlled architectures via vacuum filtration,[36,37] spin-coating,[38] or by slow evaporation.[39] The presence of extensive hydrogen-bonding interactions between the GO nanosheets enables the films to be highly stable in water once they have been dried, imparting them with exceptionally good mechanical properties and flexibility.[40] The mass production and easy processability of graphene films at low cost give this technology enormous scope ranging from environmental to medical applications. The surface coverage and material density of the synthesized GO on the substrate are important parameters to understand its efficacy for antibacterial activity. The drop-casting method followed by slow oven drying allowed the self-assembled growth of GO nanosheets, forming a coating on the well plate. The processing conditions were identical for each well plate, which enabled a similar thermal-driven layered growth of GO nanosheets along the basal plane of the microplate. This methodology adopted for GO coating on the surface was found to be a simplistic strategy to form water-stable coatings that remained intact during the antibacterial studies. This is in accordance with the literature that reports that once prepared, GO films are stable in water and show appreciable mechanical properties once they have been air dried. This could be attributed to the $\pi-\pi$ stacking and extensive H-bonding across the GO nanoparticles enabling the formation of mechanically stable films. The concentration of GO solution and other processing conditions were optimized to form homogeneous and uniform film coverage of the well plate with sufficient material density. It was observed that the intensity of color was enhanced with higher GO_I loading onto the well plate, which may be attributed to a higher solid content (Figure S1). GO loading below 60 μg led to incomplete surface coverage of the 96-well plate. Therefore, a solid content of GO in the 60−200 μg range was found to be promising and was used in the current work. The GO-coated surface containing GO_I was found to be more transparent in nature than GO_H with the same solid loading (Figure S1). The morphology of the coated films was determined by optical microscopy (Figure 1c). Optical microscopy images revealed that the GO_H coating possesses a rough surface with porous domains, whereas the use of GO_I leads to a comparatively smoother surface. This was

DOI: 10.1021/acsomega.7b00371
ACS Omega 2017, 2, 3070−3082

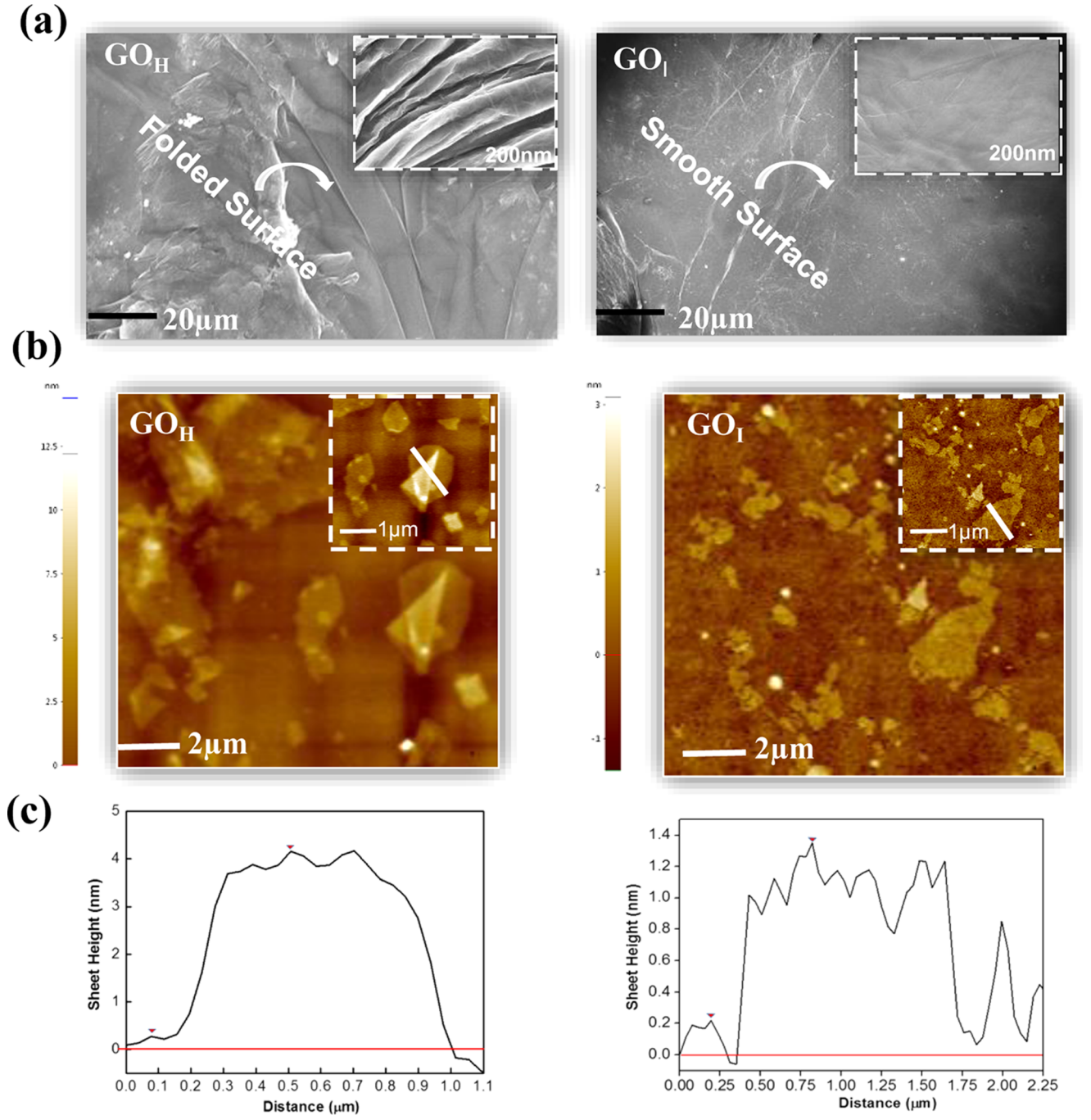

Figure 3. (a) SEM and (b) AFM images of GO_H and GO_I sheets deposited on a silicon substrate and (c) with their sheet height distribution.

further confirmed by surface thickness measurements (Table S2). As compared to that of the GO_I coating, the thickness of the GO_H coating was found to be nonhomogeneous and the difference in thickness (at edge vs. middle) was nearly 3- and 11-fold higher at 60 and 200 μg, respectively. In contrast, the GO_I coated surface was found to be uniform and had a similar thickness in all directions within the studied range of solid content.

The successful transformation of graphite to GO was confirmed by Fourier transform infrared (FT-IR) and X-ray diffraction (XRD) studies. The appearance of characteristic vibration modes due to O−H, >C═O of carboxylic acid, carbonyl, sp^2-hybridized C═C, and C−O−C epoxide functionalities at 3200, 1730, 1617, 1425, and 1050 cm^{-1}, respectively in the FT-IR spectra of both GO_H and GO_I suggest oxidation of the graphitic domains of graphite (Figure 2a). The FT-IR spectrum of GO_H exhibited a strong peak in the range 1700−1730 cm^{-1}, compared to that of GO_I, which is ascribed to carboxyl groups. The XRD patterns (Figure 2b) also support the successful oxidation of graphite to GO. There is no peak at 3.7 Å, indicating the absence of graphite flakes (starting material) in both of the GO samples. The interlayer spacing of the materials obtained from the XRD patterns is proportional to the degree of oxidation. The interlayer spacing for GO_H and GO_I was found to be 7.82 and 9.03 Å, respectively, which is indicative of the higher degree of oxidation in the latter material. To understand the nature and percentage of oxidative functionality, X-ray photoelectron spectroscopy (XPS) analysis

DOI: 10.1021/acsomega.7b00371
ACS Omega 2017, 2, 3070−3082

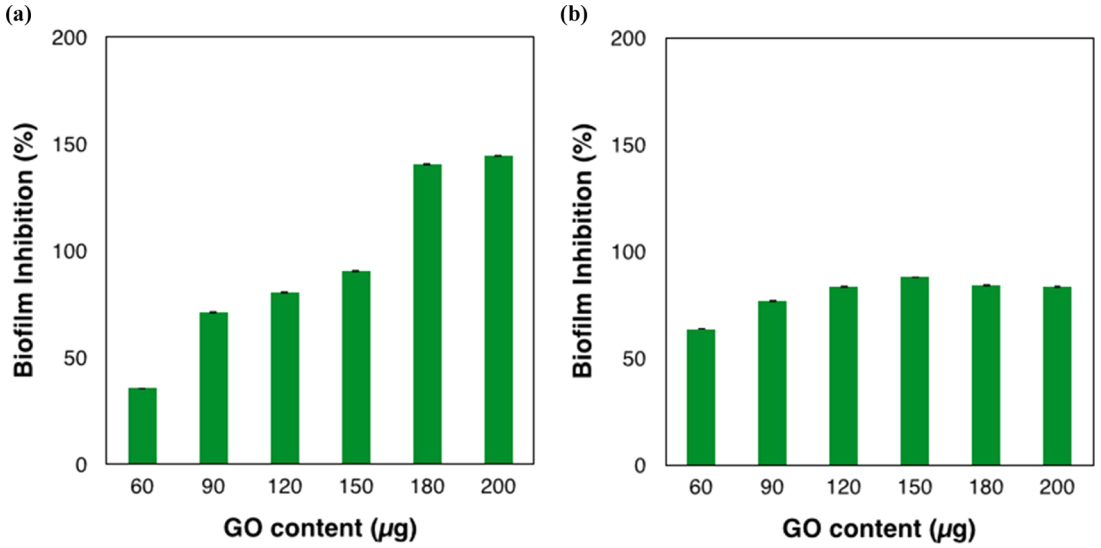

Figure 4. Antibacterial activity of GO_I-coated surface against bacterial biofilm. Quantitative analysis of bacterial biofilms after treatment of GO-coated surface with *E. coli* and *S. aureus*. Graphical representation of percentage biofilm inhibition of *E. coli* (a) and *S. aureus* (b). Data represented here shows the statistical difference (p-value < 0.05) between the GO_I-treated and control sample. Parallel experiments were also carried out on a 96-well plate without GO films, which served as a positive control.

was used to investigate the changes in the chemical states of the GO prepared by the two synthetic methods. The nature of the functional groups and their percentage was determined by deconvolution of the C 1s XPS spectra of GO_H and GO_I (Figure 2c). The C 1s core level peak of both samples was fitted according to the literature.[21] The binding energy of ∼285.0 eV was ascribed to the C═C, C−C, and C−H bonds on the surface of the sheets. The deconvoluted peaks centered at the binding energies of 286.2, 288.1, and 289.6 eV were attributed to the C−OH, epoxy, C═O, and COOH functional groups, respectively. The deconvoluted peaks suggest that both GO materials possess highly oxygenated functionalities. GO_I showed a relatively higher proportion of C−OH and epoxy-rich domains whereas GO_H has COOH groups (Table S3), which is in agreement with the FT-IR spectrum of GO_H. Both XPS and XRD patterns revealed that the relative contents of the different oxygenated groups were different in the prepared GO materials.

The surface morphology of the coated GO surfaces was studied by scanning electron microscopy (SEM). A representative SEM image of exfoliated GO_H (Figure 3a) revealed a rougher, rippled, and folded surface whereas the GO_I sheets showed a thin and smooth surface morphology. Atomic force microscopy (AFM) imaging of GO_H (Figure 3b) showed a higher thickness of ∼3.9 nm, suggesting the coexistence of multiple sheets to form a multilayered graphene architecture. The GO_I sheets exhibited an average thickness of ∼1 nm, which suggests the presence of a single-layer of exfoliated sheets. The occurrence of the higher surface roughness in GO_H can be visualized further from the 3D AFM images (Figure S2), which corroborate the optical microscopy results. Dynamic light scattering (DLS) (Figure S3) analysis indicated that the size of GO_I (200 nm) is 6-fold smaller than GO_H, suggesting larger nanoparticles in the latter material. The larger sheet size of the GO_H nanoparticles may be responsible for the observed folding and wrinkles, as indicated in the SEM and AFM analysis, which is also in agreement with the optical microscopy images.

The difference in the degree and nature of oxidation, size, and roughness of the GO prepared via the two different methodologies shows promise for exploring its potential in antimicrobial activity.

2.2. Interaction between GO and Bacterial Cells.

2.2.1. Biofilm Formation. Microbes form surface-adherent community structures called biofilms, which play a critical role in the advancement of bacterial infection. These biofilms provide antibiotic resistance and sometimes become harmful to the host immune system. Many studies have confirmed the antimicrobial activities of GO against Gram-negative bacteria. Although a plethora of data exists on the antimicrobial properties of GO sheets in suspension, not much is known about the interaction of GO-coated surfaces and bacterial cells. In this study, we have focused our attention on the use of GO-coated surfaces to prevent bacterial biofilm formation. The antibacterial activity of both synthesized GO_I- and GO_H-coated surfaces was evaluated against Gram-negative bacteria (*E. coli*) by performing a biofilm formation assay with different solid contents. Firstly, a 96-well plate was coated with different GO contents ranging from 60 to 200 μg. After this, the GO-coated plates were seeded with bacterial cells under conditions conducive for biofilm formation. Parallel experiments were also carried out on a 96-well plate without GO films that served as a positive control.

The GO synthesized via the improved method, GO_I, was found to be more effective than GO_H in inhibiting biofilm formation from Gram-negative bacteria (*E. coli*) (Figures 4a and S4). The biofilm formation percentage decreased as the content of GO_I increased, indicating the role of GO nanomaterials in the inhibition of bacterial film proliferation. However, in the case of GO_H, biofilm formation is further assisted by GO_H, as indicated by the higher optical density than that of the control (Figure S4). The biofilm inhibition percentage reached almost 90% at a GO_I content of 150 μg and even achieved over 100% at GO_I contents of 180 and 200 μg. The inhibition value did not change further on increasing the GO content, suggesting that 200 μg was the saturation limit for the *E. coli* bacterial cells. The above results are in agreement

DOI: 10.1021/acsomega.7b00371
ACS Omega 2017, 2, 3070−3082

with Perreault et al., who showed that GO-coated surfaces on cellulosic fibers at 400 μg of GO loading decreased the vitality of *E. coli* cells to a value of 30%.[18] Zou et al. reported a maximum survival rate of 20% of *E. coli* cells at a much higher thickness (~2 μm) and concentration of GO loading (>1 mg/mL) of GO films on a Whatmann polymer membrane.[24]

The effectiveness of GO_I is much higher than these reported values, which may be due to the difference in the nature of the GO and available surface area for interaction with the *E. coli* cells. The higher efficiency of the GO_I-coated surface over that of the GO_H-coated surface for bacterial growth inhibition of *E. coli* motivated us to explore the potential effect of GO_I on Gram-positive bacteria (*S. aureus*) (Figure 4b). Similarly to that for *E. coli*, GO_I also showed inhibition of *S. aureus* biofilm formation. However, GO_I was found to not be as effective as it was in the case of *E. coli*. The results indicated that biofilm inhibition was not linear with increasing GO_I content. The increase in GO_I content from 60 to 150 μg showed a marginal inhibition in biofilm formation but it was not as significant as compared to that for *E. coli*. The maximum percentage inhibition of 88% was found when using 150 μg and it was only 81% with 200 μg. As shown in the graph, the inhibition (65% vs 36%) at lower GO content (60 μg) is higher for *S. aureus* as compared to that for *E. coli*, which may be attributed to the different natures of the bacterial strains.

2.2.2. Microscopy Studies. To further confirm the anti-biofilm properties of GO, light microscopy and AFM studies were carried out to study the interaction between the GO-coated surfaces and the bacterial cells. Light microscopy images of *E. coli* and *S. aureus* at the GO_I-coated surface are shown in Figure 5. As shown in the micrographs, compact and robust biofilms were formed by *S. aureus* and *E. coli* in the control samples devoid of GO. However, only a few scattered cell aggregates can be observed in the biofilms in the presence of the GO-coated surface, as indicated by the dark domains in Figure 5. The optical microscopy images suggest a higher density of dark domains representing a higher concentration of biofilm in the case of Gram-positive *S. aureus* as compared to that of Gram-negative *E. coli*. The GO_I-coated surface is more efficient against biofilm formation of *E. coli*, which supports our biofilm formation assay results. It was observed that the methodology adopted in the deposition of the GO nanomaterial on the surface plays a significant role in the inhibition of a biofilm. Deposition of the same solid content of GO via a single step was found to be more effective as compared to that of a double-step deposition for antibacterial activity. This could be explained by assuming that one-step processing mediates the assembly of GO nanosheets in a fashion that has a higher inhibiting effect, may be due to a higher exposure of surface functionalities or morphology that avert bacterial growth.

Figure 6 shows the AFM images of biofilms of *E. coli* and *S. aureus* in the absence and presence of the GO_I-coated surface. In the absence of GO_I, the cells are spherical (*S. aureus*) and rodlike (*E.coli*), present in clusters, and compact biofilm formation was observed. Whereas, in the presence of the

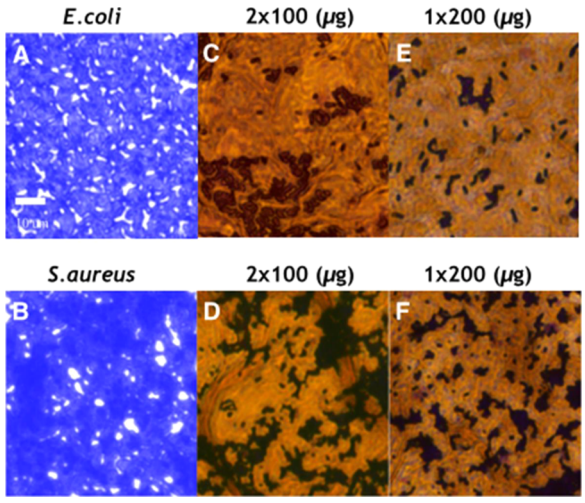

Figure 5. Light microscopy images of *E. coli* and *S. aureus* biofilms stained with crystal violet. (A, B) *E. coli* and *S. aureus* biofilms in the absence of GO_I (control). Micrographs showing biofilm inhibition in the presence of GO_I content as prepared by one-step deposition (E, F) of an aqueous dispersion of GO_I (2 mg/mL, 200 μg, 100 μL). To understand the effect of the number of depositions, the same solid content of GO_I was loaded by a double deposition (2 × 100 μg, 50 μL) onto the surface. For the double deposition, the first 50 μL sample was loaded and dried in an air oven followed by drop-casting of another 50 μL (C, D) and air drying. Scale bar = 10 μm. In the control images, the violet regions are bacterial biofilms whereas for the GO_I treated surface (C–E), the black regions are biofilms and the yellow-brown region is the GO_I nanomaterial.

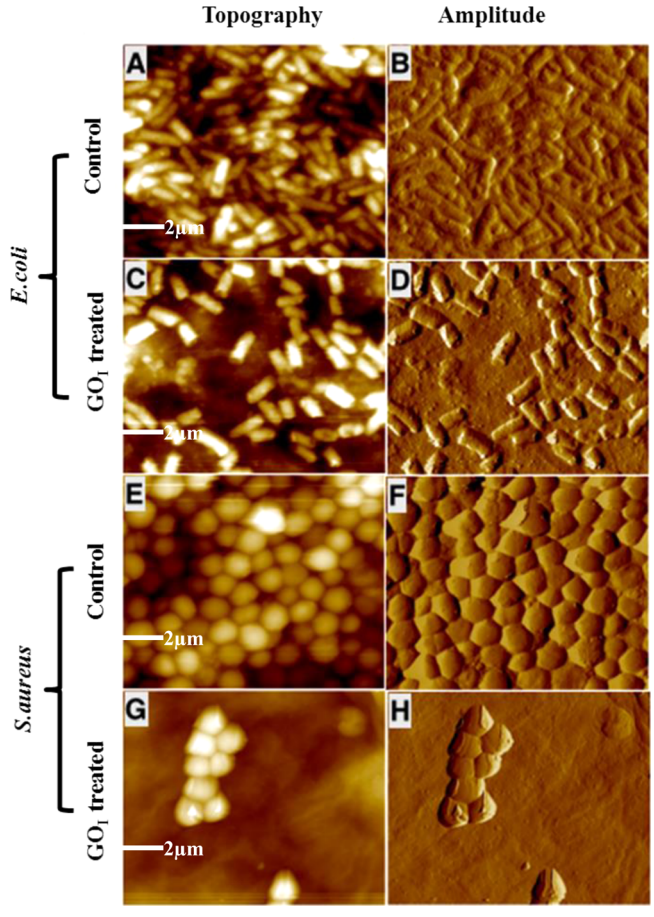

Figure 6. Representative AFM (topography and amplitude) images of *E. coli* and *S. aureus* biofilms after incubation with the GO_I (200 μg)-coated surface. Biofilm formation in the absence of GO films was taken as the positive control. (A, B) *E. coli* and (C, D) with GO_I-coated microslides; (E, F) *S. aureus* and (G, H) with GO_I-coated microslides. The microscopy images show biofilm inhibition in the presence of the same GO content of 200 μg. Scale bar = 2 μm.

DOI: 10.1021/acsomega.7b00371
ACS Omega 2017, 2, 3070–3082

GO_I-coated surface, biofilm formation decreased, as indicated by the occurrence of small cell clusters and isolated domains of biofilm and GO_I nanomaterial. The 3D AFM images of *E. coli* and *S. aureus* cells after incubation with the GO_I-coated substrate also support the existence of few-cell colonies of bacteria forming within the localized porous channels of the GO-coated substrate, and growth is not observed on the nonporous regions (Figure S5).

Biofilm formation is a multistep process involving the growth of planktonic bacteria comprising first attachment to the surface, leading to intracellular adhesion, followed by their proliferation to form cell colonies. Once such colonies reach the maturation stage, they disperse to release more cells, which then subsequently reattach to the surface to form new colonies in a similar mode.[41] In contrast to *S. aureus*, biofilm formation was greatly reduced in the case of *E. coli*, which was further indicated by the higher number of isolated cells in the AFM images (Figure 6C,D). The results from the microscopy experiments are in good agreement with our data from the biofilm formation assays. The GO_I nanomaterial was found to be effective in inhibiting biofilm formation for both strains of bacteria, Gram-positive (*S. aureus*) and Gram-negative (*E. coli*), which could be explained by several factors. The efficacy is lower in the case of *S. aureus*, which is primarily attributed to the difference in the nature of its cell wall.[42] In *S. aureus*, in addition to the presence of the cell membrane, it is further supported by a thicker peptidoglycan layer. In addition, the Gram-negative bacteria possess an additional outer membrane comprising lipopolysaccharide, which protects the peptidoglycan layer from chemical attacks. It is worth mentioning that nanoparticle-mediated toxicity toward bacterial species not only relies on the bacterial structure but also depends on several factors including the enzymatic activity.[43]

It is worth noting that during the establishment of biofilm formation, the bacterial cells become embedded in the energy-rich self-produced extracellular polymeric matrix comprising polysaccharides, proteins, lipids, and nucleic acids.[44] Signaling across the bacterial network promotes genetic growth in response to favorable environmental conditions allowing the transition between the free planktonic state to surface-attached cells and their further proliferation. In order for the occurrence of such a growth mechanism, generation of a foothold by the bacteria on the surface is a mandatory requirement to mediate cell-to-cell and cell-to-surface interactions with the support of a nutrient supply to develop bacterial structural scaffolds. If the surface is not supportive and is antiadhesive to such growth of the biofilm either chemically or physically, this will be key to preventing such undesirable bacterial colonization.

Considering the material perspective, the antibacterial properties of GO are associated with inherent or structurally modified chemical and physical factors. Some studies based on suspensions of GO particles have suggested that the sharp edges of GO sheets penetrate and puncture the cell membrane leading to cell death via leakage of cytoplasmic materials. In our case, the nanosheets of the GO material are not in suspension but rather they are coated on the substrate. It is expected that the slow evaporation of aqueous media leads to a self-assembled nano-layer coated surface where the majority of the sheets lie flat in the basal plane of the surface of the substrate. The profilometry and morphology studies indicate the formation of thinner and more uniform packed sheets in the case of GO_I than that of GO_H, which is due to their smaller sheet size. It is anticipated that at lower solid loadings of GO, there will be fewer sharp edges than at those at higher loadings, which may account for the cell death due to penetration and rupturing of the cell membrane. The SEM images showed a wrinkled/folded surface for GO_H, whereas the surface is smooth for GO_I, implying minimal or insignificant physical destruction due to nanomaterial edges in the latter. The presence of the smooth surface may not provide sufficiently attractive surface properties for anchoring of bacteria thereby interfering with the cell−surface interactions and inhibiting bacterial attachment, which is the primary requirement for the establishment of a biofilm. The GO-uncoated control surface showed intricate bacteria densely embedded in the matrix; the development of thick, dense biofilms that uniformly covered the surfaces. From our results, the morphologies of the GO_H and GO_I surfaces differed significantly in terms of their porous framework and surface roughness on the physical front, and chemically in terms of their surface functionalities. In this case, one may argue that the GO_H surface possesses a modest rough surface, which is conducive to the formation of a bacterial foothold and may promote biofilm formation by facilitating the anchoring mechanism. On the contrary, the GO_I-coated surface was smooth, which may have prevented the adhesion of bacteria to a moderate level, allowing the initial aggregation of bacteria only at the place of seeding the colony, which mediate the growth locally creating a partially covered surface, however further growth is inhibited.

2.2.3. CA Measurements. To understand the importance of the surface−interface interactions of the GO-coated substrate, further detailed study in this direction is necessary. The key dictating parameters for surfaces to mitigate attachment and proliferation of bacteria on an anti-biofouling surface are the surface free energy, wettability,[30,31] elasticity, surface topography in terms of pore size and their density,[45] and surface roughness.[24] Simultaneously, the nature of and surface charge on bacteria also play a crucial role in facilitating their electrostatic and hydrophobic interactions with an anti-biofouling surface, controlling their growth.[30,31] It has been reported that depending upon the species of bacteria and ionic strength of a medium, the surface properties of the bacteria may change. Both hydrophilic and hydrophobic interactions play a significant role in attachment of bacteria to any surface. The surface properties of graphene-coated substrates against biofouling have been immensely studied by Parra et al.[30,31] They demonstrated that the surface properties of graphene-coated metallic substrates are important for understanding the mechanistic aspect of biofilm formation. Such graphene coatings modify the material's surface energy via hydrophobic−hydrophilic and electrostatic interactions between the coated material and bacteria, which is essential for imparting anti-biofouling characteristics. The graphene surface provides an effective barrier thereby preventing physical contact between the bacteria and underlying substrate to substantially suppress interaction, which is an essential requirement for the establishment of the biofilm. An antibacterial activity study of graphene coated on gold and copper substrates demonstrated that graphene conductivity plays no role in bacterial viability, rather the release of cupric ions is responsible for the bactericidal affect.[32]

To understand the importance of surface energies for anti-biofouling properties, CA measurements on GO_H/GO_I-coated substrates was performed (Figure S6). The GO_H and GO_I surfaces showed a CA of ∼33 and ∼46°, respectively, suggesting the former is more hydrophilic in nature. This is

DOI: 10.1021/acsomega.7b00371
ACS Omega 2017, 2, 3070−3082

also in good agreement with our XPS results (Table S3), as the former possesses a larger number of more hydrophilic carboxylic functionalities.

The GO_I-coated substrate being more hydrophobic in nature than that with GO_H should favor the growth of a bacterial biofilm that possesses a hydrophobic surface such as *E. coli*. However, the results suggest there are some other factors too. The bioadhesive material released from bacteria is a complex mixture of polysaccharides along with proteins that possess both hydrophobic and hydrophilic properties leading to an aqueous gellike network.[46] The ratio of these constituents may vary amongst bacterial species. It is anticipated that the different surface energies of the GO_H- and GO_I-coated substrates may be playing a significant role in the spread of the released adhesive glue[31] by bacteria across their surfaces, which is essential for biofilm formation. Biofilm formation is a complex process and is dictated by a variety of physicochemical and biological factors at the interface of the cell and surface of the substrate, facilitating cell attachment, microcolony formation, and the release of adhesive glue followed by release of planktonic cells.

In comparison to that of GO_H, the surface properties of the GO_I-coated substrate are not cooperative with bacterial biofilm formation, and may affect the interactions of the cell with the surface and inhibit the initial bacterial attachment, which is the primary requirement for biofilm establishment. However, where some cell attachment succeeded, it was not allowing to further grow. This could be explained in chemical terms, as the released bacterial adhesive, which is essential for the spread of bacteria, may undergo some chemical modification due to the different surface functionalities on the GO_I surface affecting proliferation. Simultaneously, physical barriers may counter biofilm development by affecting the abiotic surface binding energies and inter-/intra-cellular adhesive/cohesive forces that are dependent on porosity[45] and the surface energy of the substrate.[30,31]

2.2.4. Oxidative Stress Studies. Besides the physical parameters, chemical factors such as the generation of ROS believed to enhance oxidative stress, which is responsible for toxicity due to cellular oxidation of molecules, may lead to cell death. The oxidative stress in bacterial cells is minimized by a self-defense mechanism involving the redox reaction of thiol/sulfhydryl groups (−SH) present in glutathione (GSH) to form glutathione disulfide (GSSG). The concentration of GSH in the cell plays a significant role in negating such stresses. Carbon nanomaterials,[47] such as fullerene,[48] CNTs,[16] and GO,[21] are known to enhance ROS species inside the cell. The oxidation of glutathione by GO can occur either via the direct oxidation of biomolecules by GO sheets or the adsorption of oxygen on defect sites or through oxidizable functionalities leading to the formation of the graphene structure. Even reduced graphene has exhibited a higher loss of glutathione, which is explained by superoxide anion-independent oxidative stress due to its conducting nature.[19] The intercalation of water molecules at the graphene surface has been shown to generate hydroxyl radical species that support the ROS mechanism involving attack on peptide linkages with the simultaneous destruction of the cell wall of bacteria.[49] The density of functional groups, size, and conductivity plays a crucial role in generating such stress hampering of cell growth. The sheet size reduction of GO has been reported to cause a higher percentage of loss of glutathione.[18] The oxidative stress due to ROS can be determined by oxidant-sensitive dye 2′,7′-dichlorofluorescein diacetate assay,[50] nitro blue tetrazolium reduction assay,[51] and more commonly by Ellman's assay. GO can therefore lead to oxidative stress in the presence of oxygen and cellular antioxidants, either by formation of ROS or by the depletion of cellular antioxidants. To confirm whether a similar mechanism was occurring on the GO-coated surface and may be responsible for the inhibition of biofilms, we studied the oxidative stress mediated by the GO-coated surface on the well plate. The amount of free thiol groups due to GSH present in the cell was investigated by Ellman's reagent, which is a water-soluble colorimetric reagent, which upon reaction with free thiol moieties forms a yellow-colored product, 2-nitro-5-thiobenzoic acid (NTB), which can be measured at 412 nm by UV−visible spectroscopy. Here, a bicarbonate buffer (50 mM) was used as a negative control and because H_2O_2 (1 mM) induces ROS, it was employed as a positive control. The amount of oxidative stress generated by the GO_I surface was quantified and is shown in Figure 7, wherein glutathione

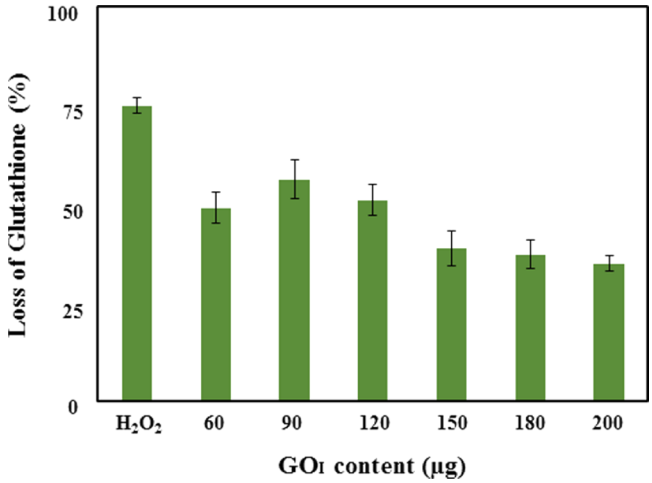

Figure 7. Oxidative stress induced by GO_I-coated surface. Loss of glutathione percentage after in vitro incubation with the GO films at different GO contents ranging from 60 to 200 μg for 3 h. A bicarbonate buffer without a GO film was taken as the negative control and H_2O_2 was used as a positive control. Data represented here for glutathione oxidation between the treated and control samples was found to be statistically significant (p-value < 0.05).

percentage decreased with increasing GO content coated on the well plate. The oxidation of GSH by graphene-based materials in suspension has been known to increase with increasing concentration to generate more oxidative stress toward bacterial cells.[19] In our case, as GO_I content increased from 60 to 90 μg, the percentage loss of glutathione increased from 50 to 60%, which may be due to a higher GO content leading to higher ROS-mediated oxidative stress, as expected. Surprisingly, as the GO content increased further, the loss of glutathione decreased to a value of 35% at 200 μg. The oxidative stress due to the GO coating is dictated both by GO content and availability of exposed surface functionalities. Therefore, oxidative stress was found to increase with increasing GO content from 60 to 90 μg. However, with the further increase in GO content to 200 μg, a decrease in oxidative stress is observed. The reason for this decrease in oxidation potential of GO beyond a certain loading (i.e., 90 μg) may be attributed to the non-accessibility of initially deposited GO sheets due to the higher loading of GO content on top of it. In addition, it may involve some of the surface functionalities

DOI: 10.1021/acsomega.7b00371
ACS Omega 2017, 2, 3070−3082

undergoing inter/intramolecular H-bonding amongst GO nanoparticles leading to the formation of a thicker layer at higher GO content. Therefore with a higher loading (> 90 μg) of more GO nanosheets, both of these processes may be responsible for the reduction in GSH oxidation. Seemingly, besides other probable reasons for the antibacterial activity, the GO-coated sheets also exhibited the potential to create oxidative stress on the bacterial cells as in suspension. To further support our hypothesis of the ineffectiveness of the initially deposited GO sheets due to further GO loading, Ellman's assay was performed in a GO suspension. Figure S7 shows that loss of glutathione was found to be dependent on GO_I content; the value increases with increasing GO concentration in the suspension, which is in agreement with the literature. The percentage loss of GSH is similar at lower GO_I content (~50−60 μg) both for the coating and suspension confirming the availability of similar surface functionalities and density of states to oxidize GSH. However, at higher GO_I content (~90−100 μg), the suspension showed nearly 20% higher loss of glutathione than that of the coated nanomaterial supporting our hypothesis that there is more exposure to and interaction of the GO surface with the bacteria in suspension than that as a coating on the substrate. In addition, at 100 μg/mL, both GO_I and GO_H dispersions showed a similar percentage loss of GSH, 77 and 76%, respectively. This suggests that irrespective of the nature of the synthetic route adopted in the synthesis, both GO_H and GO_I will cause similar oxidative stress to the bacterial cells.

It has been reported that the sheet size of GO dictates the extent of glutathione oxidation, that is, a smaller sheet size leads to a higher oxidation potential.[18] Chemically, it is expected that carboxylic groups possess a greater oxidation capability than that of epoxy and hydroxyl groups. Therefore, it is worth mentioning that even though the nature and degree of oxygenated functionalities are different for GO_I (epoxide- and hydroxyl-rich) and GO_H (carboxyl-rich), the possibility of oxidation of glutathione or substantial adsorption of both water and oxygen molecules to mediate oxidative stress must also be taken into account. Therefore, oxidative stress-induced bacterial cell inhibition may not be a predominant mechanism in dictating bacterial proliferation and cell death.

2.2.5. Antimicrobial Effect of GO in Dispersions. Further, the antibacterial activity of GO dispersions prepared by the two methods against both *E. coli* and *S. aureus* at the same concentration (50 and 100 μg/mL) in suspension was also determined using the CFU method (Figure S8). The results revealed that both GO_I and GO_H are selective in their antibacterial activity. GO_I inhibits *E. coli* (77 and 85%) and *S. aureus* (44 and 52%) at 50 and 100 μg/mL, respectively. Whereas, GO_H inhibits *E. coli* (49 and 66%) and *S. aureus* (84 and 93%) at 50 and 100 μg/mL, respectively. The results were further supported by spot analysis (Figure S9), which showed similar results. GO_H showed a pronounced antibacterial activity against *S. aureus*. As both GO_H and GO_I have similar oxidative stress, as determined by Ellman's assay, it may be the size of the nanoparticles that dictates the selective killing of cells. DLS studies revealed a smaller hydrodynamic radii of GO_I (200 nm) than that of GO_H (1200 nm), as shown in Figure S3. This suggests that the mechanism of inhibitory effect of GO_I is via piercing the thin cell wall in *E. coli* cells. However, the thicker cell wall in *S. aureus* is difficult to pierce by GO_I and therefore wrapping of the bacterial cells by larger sheets of GO_H is the predominant mechanism to lower its population. In the suspension studies, the effect of GO may be more bacteriostatic than bactericidal as the percentage of inhibition observed was below 99.99%.

The above experiments assist us in stating that bacterial biofilm formation is mainly inhibited by the surface morphology of GO-coated substrates, as dictated by the porosity and surface roughness. However, an ROS-mediated mechanism plays a limited role in preventing biofilm formation.

3. CONCLUSIONS

In summary, syntheses of GO via an improved and traditional Hummers' method were carried out and the fabrication of a GO-coated surface on a well plate was optimized and demonstrated to be efficient in preventing biofilm formation. The GO_I nanosheet possesses epoxide- and hydroxyl-rich surface functionalities and a smaller size whereas that of GO_H is dominated by carboxylic-rich groups and a larger sheet size. The analysis of the coated surfaces revealed a smooth, less porous, thinner film in the case of GO_I, which enhances its inhibition of bacterial biofilm formation of the model bacterium *E. coli*. On the contrary, adhesion of bacterial cells is promoted by the higher surface roughness and non-uniform thickness of the GO_H-coated surface. The mechanism for such inhibition was further supported by microscopy and loss of GSH studies. Further understanding of the inhibitory effect on bacterial proliferation showed a selective inhibitory effect of the GO nanoparticles. GO_H showed a pronounced inhibiting effect on *S. aureus* whereas GO_I is more selective toward the *E. coli* population. In response to environmental cues, bacterial cells promote gene transcription that facilitates the transition between free planktonic states and surface-attached cells. Cell-to-cell and cell-to-surface interactions play an important role in biofilm establishment. Bacteria adhere to the surface by a fibrillary structure such as fimbriae or pili during biofilm formation. It is probable that in the presence of GO, any one or more of these complex processes is disturbed leading to a decrease in biofilm formation. The current findings on GO surfaces preventing biofilm formation are expected to have immediate implications in their design and utility for commercial applications, especially within the health care sector.

4. MATERIALS AND METHODS

4.1. Preparation and Characterization of GO. Graphite flakes [Alfa Aesar, 99.8%, natural graphite (325 mesh)], sulfuric acid (Finar), sodium nitrate, potassium permanganate, orthophosphoric acid, and hydrogen peroxide [30% (w/w)] were obtained from Fisher scientific. All reagents were used as received.

FT-IR spectra were recorded on a Nicolet iS5 spectrometer equipped with an iD5-ATR accessory, in the range of 4000−400 cm^{-1} with a resolution of 4 cm^{-1}. Absorbance measurements were carried out on a Thermo Scientific Evolution 201 UV−visible spectrophotometer by preparing dispersions of the respective nanomaterial in deionized water. X-ray diffraction studies were performed on a Rigaku SmartLab X-ray Diffractometer with Cu Kα radiation (λ = 1.5406 Å). The surface morphology of the samples was studied using a scanning electron microscope (Zeiss EVO MA15) under an acceleration voltage of 1 kV. Samples were mounted on aluminum stubs and sputter-coated with gold and palladium (10 nm) using a sputter coater (Quorum-SC7620) operating at

DOI: 10.1021/acsomega.7b00371
ACS Omega 2017, 2, 3070−3082

10−12 mA for 120 s. AFM (PARK, XE-007) in noncontact mode was used to detect the morphology and thickness of GO. The average particle size of the particles was measured by DLS (Nanosizer, Malvern, U.K.). XPS (Omicron Multiprobe Surface Analysis System) measurements using a monochromatized Al Kα (1486.7 eV) radiation source were carried out to analyze the surface chemistry of GO. Contact angle (CA) measurements were performed to characterize the surface properties of the GO-coated polystyrene (PS) substrates on a CA system (Krüss GmbH, DSA-25). A drop of milliQ water (2 μL) was placed on the surface of the GO-coated and uncoated PS sample and images were immediately captured using a CCD camera equipped with a magnifying lens. To confirm the repeatability of the recorded data, measurements at different positions on each sample were recorded and errors were found to be within $\pm$ 2°. A surface profilometer (Bruker, Dektak XT) was used to measure the surface thickness of the GO-coated surfaces. Centrifugation was carried out using an Eppendorf 5810R (25 °C, 9000 rpm, 20 min for each centrifugation cycle). Evaporation of the solvent from the GO suspension was performed using a Heidolph rotavac (122 rpm, ∼60 °C). A probe sonicator (Sonics USA; 500 W, 20 kHz) was used at 40% max. amplitude with a pulse time of 10 s. A Thermofisher air oven (HERA therm) was used to make the GO film on the 96-well plate.

Graphite flakes were oxidized using two different procedures, namely, Hummers' method and an improved method to prepare GO_H and GO_I, respectively. For the Hummers' method,[34] graphite flakes (1.0 g, 1.0 wt equiv) were added to a mixture of concentrated sulfuric acid (23.0 mL) and sodium nitrate (0.5 g, 0.5 wt equiv) while keeping the temperature at 0 °C with continuous stirring. This was followed by a gradual addition of potassium permanganate (3.0 g, 3.0 wt equiv) while maintaining the temperature below 20 °C. Upon completion of the addition, the ice bath was removed and the resultant suspension was stirred. The mixture turned to a brownish gray color in 30 min after which distilled water (46 mL) was added. The solution was finally treated with warm water (140 mL) and hydrogen peroxide (30% w/w, 3 mL) to give a brown colored GO. The formed GO was washed, redispersed in water, and then centrifuged (9000 rpm for 20 min) until the pH of the suspension was found to be neutral. The residue obtained was dried under vacuum to yield a brown solid (0.82 g, GO_H). For the improved method (methodology was followed from a reported procedure by Marcano et al.[35] with slight modifications), a mixture of concentrated sulfuric acid/phosphoric acid (134 mL, 8.6:1) was added to a mixture of graphite flakes (1.0 g, 1.0 wt equiv) with stirring at room temperature. To this, potassium permanganate (6.0 g, 6.0 wt equiv) was slowly added with the production of a slight exotherm to 45 °C. After the addition, the reaction mixture was heated to 50 °C and stirred for a further 12 h. The reaction mixture was allowed to cool to room temperature. Under stirring, a mixture of ice cold water/H_2O_2 (250:3 mL) was added slowly. During the addition, a noticeable color change was observed from dark brown to yellow. The reaction mixture was allowed to settle under gravity and the supernatant was decanted. The residue formed was washed, redispersed in water, and then centrifuged (9000 rpm for 20 min) and the process was repeated until the pH of the dispersion was found to be neutral. The resulting suspended material obtained after a multiple-wash process was dried in a rotary evaporator at 50 °C under vacuum to yield a light brown solid (2.30 g, GO_I).

4.2. Deposition of GO. A respective GO_H/GO_I suspension was prepared in double deionized water with a stock concentration of 2 mg/mL. Then, the suspension was sonicated using a probe sonicator for 2 min before drop-casting the solution on a 96-well microtiter flat bottom plate. Thereafter, the suspension was slowly dried in an air oven at 50 °C for 4 h to obtain the GO-coated wells. A series of different GO contents in triplicate were loaded onto the well plate and details of the volumes used are given in Table S1.

4.3. Bacterial Strains and Culture Conditions. *E. coli* (MG1655) and *S. aureus* were grown overnight at 37 °C in Luria bertani (LB) and tryptic soy broth (TSB), respectively. Culture media (TSB and LB), glucose, and acetic acid were obtained from Himedia, Mumbai. Crystal violet was obtained from Sigma-Aldrich (St. Louis, MO). All bacterial cultures were grown at 37 °C in aerobic conditions.

4.4. Antimicrobial Activity of GO-Coated Surfaces toward Biofilm Formation Assay. To examine the antibacterial activity of the GO-coated surface, the biofilm formation percentage of *E. coli* and *S. aureus* was determined using the 96-well microtiter plate[52] coated with the GO surface. Wells coated with GO served as the test and uncoated wells were taken as the control. The overnight grown bacterial culture was diluted by 1:100 in fresh TSB (*S. aureus*) and LB (*E. coli*) media supplemented with 2% glucose. After 24 h, planktonic cells were removed gently and wells were washed thrice with distilled water. Biofilms formed on coated GO were stained with 0.2% crystal violet solution and again washed with distilled water. Acetic acid, 30%, was used for biofilm quantification and the optical density at 595 nm was determined using an i-Mark Microplate reader (Bio-Rad).

4.5. Microscopy. For AFM, biofilms were grown on coverslips coated with GO, after 24 h, planktonic cells were removed gently by rinsing the coverslips three times in distilled water. When dry, the coverslips were imaged directly under AFM using tapping mode. For light microscopy, a 24-well PS plate coated with a GO content of 200 μg was used. After staining the biofilms with crystal violet, wells were washed with distilled water. When the plates were dried, light microscopy of the stained biofilms was performed by a Leica (DMIL LED Model) using 40× objective. The same microscope was used to record the microscopy image of the GO-coated surface.

4.6. Ellman's Assay. Thiol oxidation by GO as a coating and as suspension was determined using Ellman's reagent [Alfa aesar, 5,5′-dithiobis(2-nitrobenzoic acid)] under acellular conditions. Reduced glutathione (0.8 mM) was exposed to the coated GO surface with different GO contents (60−200 μg) in a bicarbonate buffer (pH 8.6). Samples were incubated at room temperature for 3 h in the dark. For dispersion analysis, GO_H and GO_I at concentrations of 50 μg/mL and 100 μg/mL in 50 mM bicarbonate buffer were incubated with 0.8 mM glutathione for 3 h at 150 rpm in the dark. After incubation, the amount of nonoxidized glutathione (GSH) was quantified spectrophotometrically at 412 nm by adding 0.05 mM TrisCl and 100 mM Ellman's reagent, which reacts with the thiol groups of GSH to yield NTB. A GSH solution without GO was used as the negative control whereas GSH oxidation by hydrogen peroxide (1 mM) was used as the positive control in the following experiments. The loss of GSH was evaluated using the equation below

DOI: 10.1021/acsomega.7b00371
ACS Omega 2017, 2, 3070−3082

$$\text{loss of GSH (\%)} = \frac{\text{absorbance of negative control} - \text{absorbance of sample}}{\text{absorbance of negative control}} \times 100$$

4.7. Cell Viability Test. We studied the antibacterial activity of GO_H and GO_I against *E. coli* and *S. aureus*. Cells at 10^7 CFU/mL were used to determine antibacterial activity. Briefly, 50 μg/mL and 100 μg/mL of GO_H or GO_I (probe sonication for 2 min) were incubated with the bacterial cell suspensions and kept at 200 rpm to ensure proper contact. Parallel experiments were also conducted with bacterial cell suspensions without any compound to serve as the positive control. After 24 h, 100 μL of the cell suspension was 10-fold serially diluted and spread on an agar plate. The antimicrobial activity of GO was evaluated by CFU and expressed in terms of percentage inhibition.

For spot assay, overnight grown cultures of *E. coli* and *S. aureus* were harvested and washed with saline to remove the medium and macromolecules. The bacterial cell suspension was then diluted to obtain 10^7 CFU/mL and the cells were treated with 50 and 100 μg/mL of GO_H or GO_I (probe sonication for 2 min), untreated cells were taken as the control. Both treated and untreated cells were allowed to grow for 24 h at 37 °C and 200 rpm. After 24 h, serial dilutions of the treated and control samples were performed and 5 μL was spotted on agar plates. Plates were incubated overnight at 37 °C and digital images were recorded.

4.8. Statistical Analysis. For all of the graphical experiments, analysis of variance was used to evaluate the significant differences. The p-value was found to be <0.05 for all of the experiments.

■ ASSOCIATED CONTENT

Supporting Information

The Supporting Information is available free of charge on the ACS Publications website at DOI: 10.1021/acsomega.7b00371.

Digital images of GO-coated well plates of different GO solid content loadings; AFM (3D) images of GO_H and GO_I films and representative height distribution; hydrodynamic mean diameter and size distribution of GO_H and GO_I; quantitative analysis of antibacterial activity of GO_H-coated surface against *E. coli* bacterial biofilm formation; 3D AFM images of *E. coli* and *S. aureus* cells after incubation with GO_I-coated substrate; images of CA measurements using MilliQ water in contact with (a) PS substrate (control), (b) GO_H coated on PS, and (c) GO_I coated on PS; in vitro glutathione oxidation induced by GO nanomaterials; antimicrobial activity of GO_H and GO_I with different concentrations; spot assay representing antimicrobial activity of GO_I and GO_H; methodology adopted for preparation of different GO solid contents onto 96-well plate; surface thickness measurements of GO_H- and GO_I-coated surface; XRD data (d—interlayer spacing) and XPS deconvoluted percentage component of GO_H and GO_I; comparison of our GO-coated substrate with previously reported literature (PDF)

■ AUTHOR INFORMATION

Corresponding Authors

*E-mail: richa.priyadarshini@snu.edu.in (R.P.).
*E-mail: bimlesh.lochab@snu.edu.in (B.L.).

ORCID

Bimlesh Lochab: 0000-0002-8434-6513

Author Contributions

The manuscript was written through contributions of N.Y., A.D., S.S., R.P., and B.L. and C.P.S. assisted in recording the AFM images and surface thickness measurements. G.G. assisted in recording and analyzing XPS data. All authors have given approval to the final version of the manuscript.

Notes

The authors declare no competing financial interest.

■ ACKNOWLEDGMENTS

This work was financially supported by Shiv Nadar University. The authors would like to acknowledge Prof. Aloke Kanjilal for allowing the use of the CA instrument that was purchased through the Alexander von Humboldt Foundation.

■ REFERENCES

(1) Novoselov, K. S.; Geim, A. K.; Morozov, S. V.; Jiang, D.; Zhang, Y.; Dubonos, S. V.; Grigorieva, I. V.; Firsov, A. A. Electric Field Effect in Atomically Thin Carbon Films. *Science* **2004**, *306*, 666−669.

(2) Mkhoyan, K.; Contryman, A.; Silcox, J.; Stewart, D.; Eda, G.; Mattevi, C.; Miller, S.; Chhowalla, M. Atomic and Electronic Structure of Graphene-Oxide. *NanoLett.* **2009**, *9*, 1058−1063.

(3) Lerf, A.; He, H.; Forster, M.; Klinowski, J. Structure of Graphite Oxide Revisited. *J. Phys. Chem. B* **1998**, *102*, 4477−4482.

(4) Krishnamoorthy, K.; Veerapandian, M.; Zhang, L. H.; Yun, K.; Kim, S. J. Antibacterial Efficiency of Graphene Nanosheets against Pathogenic Bacteria via Lipid Peroxidation. *J. Phys. Chem. C* **2012**, *116*, 17280−17287.

(5) Cha, C.; Shin, S. R.; Annabi, N.; Dokmeci, M. R.; Khademhosseini, A. Carbon-Based Nanomaterials: Multi-Functional Materials for Biomedical Engineering. *ACS Nano* **2013**, *7*, 2891−2897.

(6) Yang, K.; Zhang, S.; Zhang, G.; Sun, X.; Lee, S.-T.; Liu, Z. Graphene in Mice: Ultrahigh in Vivo Tumor Uptake and Efficient Photothermal Therapy. *Nano Lett.* **2010**, *10*, 3318−3323.

(7) Feng, L.; Liu, Z. A. Graphene in Biomedicine: Opportunities and Challenges. *Nanomedicine* **2011**, *6*, 317−324.

(8) Moran, A.; Israela, B.; Ziberman, M. Gentamicin-Loaded Bioresorbable Films for Prevention of Bacterial Infections Associated with Orthopedic Implants. *J. Biomed. Mater. Res., Part A* **2007**, *83A*, 10−19.

(9) Levy, S. B.; Marshall, B. Antibacterial Resistance Worldwide: Causes, Challenges and Responses. *Nat. Med.* **2002**, *12*, 122−129.

(10) Kumar, A.; Vemula, P. K.; Ajayan, P. M.; John, G. Silver-Nanoparticle-Embedded Antimicrobial Paints Based on Vegetable Oil. *Nat. Mater.* **2008**, *7*, 236−241.

(11) Payne, J. N.; Waghwani, H. K.; Connor, M. J.; Hamilton, W.; Tockstein, S.; Moolani, H.; Chavda, F.; Badwaik, V.; Lawrenz, M. B.; Dakshinamurthy, R. Novel Synthesis of Kanamycin Conjugated Gold Nanoparticles with Potent Antibacterial Activity. *Front. Microbiol.* **2016**, *7*, 607.

(12) Bataillon, S. B.; Tattevin, P.; Mallet, M. B.; Gougeon, A. J. Emergence of Resistance to Antibacterial agents: the Role of Quaternary Ammonium Compounds - A Critical Review. *Int. J. Antimicrob. Agents* **2012**, *39*, 381−389.

(13) Akhavan, O.; Ghaderi, E. Toxicity of Graphene and Graphene Oxide Nanowalls against Bacteria. *ACS Nano* **2010**, *4*, 5731−5736.

(14) Lyon, D. Y.; Adams, L. K.; Falkner, J. C.; Alvarez, P. J. J. Antibacterial Activity of Fullerene Water Suspensions: Effects of Preparation Method and Particle Size. *Environ. Sci. Technol.* **2006**, *40*, 4360−4366.

(15) Kang, S.; Herzberg, M.; Rodrigues, D. F.; Elimelech, M. Antibacterial Effects of Carbon Nanotubes: Size Does Matter. *Langmuir* **2008**, *24*, 6409−6413.

DOI: 10.1021/acsomega.7b00371
ACS Omega 2017, 2, 3070−3082

(16) Vecitis, C. D.; Zodrow, K. R.; Kang, S.; Elimelech, M. Electronic-Structure-Dependent Bacterial Cytotoxicity of Single-Walled Carbon Nanotubes. *ACS Nano* **2010**, *4*, 5471−5479.
(17) Tu, Y.; Lv, M.; Xiu, P.; Huynh, T.; Zhang, M.; Castelli, M.; Liu, Z.; Huang, Q.; Fan, C.; Fang, H.; Zhou, R. Destructive Extraction of Phospholipids from *Escherichia coli* Membranes by Graphene Nanosheets. *Nat. Nanotechnol.* **2013**, *8*, 594−60.
(18) Perreault, F.; de Faria, A. F.; Nejati, S.; Elimelech, M. Antimicrobial Properties of Graphene Oxide Nanosheets: Why Size Matters. *ACS Nano* **2015**, *9*, 7226−7236.
(19) Liu, S.; Zeng, T. H.; Hofmann, M.; Burcombe, E.; Wei, J.; Jiang, R.; Kong, J.; Chen, Y. Antibacterial activity of Graphite, Graphite Oxide, Graphene Oxide, and Reduced Graphene Oxide: Membrane and Oxidative Stress. *ACS Nano* **2011**, *5*, 6971−6980.
(20) Wang, X.; Quinn, P. J. Vitamin E and its Function in Membranes. *Prog. Lipid Res.* **1999**, *38*, 309−336.
(21) Liu, S.; Hu, M.; Zeng, T. H.; Wu, R.; Jiang, R.; Wei, J.; Wang, L.; Kong, J.; Chen, Y. Lateral Dimension-Dependent Antibacterial Activity of Graphene Oxide Sheets. *Langmuir* **2012**, *28*, 12364−12372.
(22) Pham, V. T. H.; Truong, V. K.; Quinn, M. D. J.; Notley, S. M.; Guo, Y.; Baulin, V. A.; Kobaisi, M. A.; Crawford, R. J.; Ivanova, E. P. Graphene Induces Formation of Pores that Kill Spherical and Rod-Shaped Bacteria. *ACS Nano* **2015**, *9*, 8458−8467.
(23) Hu, W.; Peng, C.; Luo, W.; Lv, M.; Li, X.; Li, D.; Huang, Q.; Fan, C. Graphene based Antibacterial Paper. *ACS Nano* **2010**, *4*, 4317−4323.
(24) Zou, F.; Zhou, H.; Jeong, D. Y.; Kwon, J.; Eom, S. U.; Park, T. J.; Hong, S. W.; Lee, J. Wrinkled Surface-Mediated Antibacterial Activity of Graphene Oxide Nanosheets. *ACS Appl. Mater. Interfaces* **2017**, *9*, 1343−1351.
(25) Costerton, J. W.; Stewart, P. S.; Greenberg, E. P. Bacterial Biofilms: A Common Cause of Persistent Infections. *Science* **1999**, *284*, 1318−1322.
(26) Donlan, R. M.; Costerton, J. W. Biofilms: Survival Mechanisms of Clinically Relevant Microorganisms. *Clin. Microbiol. Rev.* **2002**, *15*, 167−193.
(27) Klevens, R. M.; Morrison, M. A.; Nadle, J.; et al. Invasive Methicillin-Resistant Staphylococcus aureus Infections in the United States. *J. Am. Med. Assoc.* **2007**, *298*, 1763−1771.
(28) Johnson, J. R. Virulence factors in *Escherichia coli* Urinary Tract Infection. *Clin. Microbiol. Rev.* **1991**, *4*, 80−128.
(29) Soto, S. M.; Smithson, A.; Martinez, J. A.; Horcajada, J. P.; Mensa, J.; Vila, J. Biofilm formation in Uropathogenic *Escherichia coli* Strains: Relationship with Prostatitis, Urovirulence factors and Antimicrobial Resistance. *J. Urol.* **2007**, *177*, 365−368.
(30) Parra, C.; Silva, F. M.; Henríquez, R.; Flores, M.; Garín, C.; Ramírez, C.; Moreno, M.; Correa, J.; Seeger, M.; Häberle, P. Suppressing Interaction with Copper Surfaces through Graphene and Hexagonal-Boron Nitride Coatings. *ACS Appl. Mater. Interfaces* **2015**, *7*, 6430−6437.
(31) Parra, C.; Dorta, F.; Jimenez, E.; Henríquez, R.; Ramirez, C.; Rojas, R.; Villalbos, P. Nanomolecular Approach to Decrease Adhesion of Biofouling-producing Bacteria to Graphene-Coated. *J. Nanobiotechnol.* **2015**, *13*, 82−91.
(32) Dellieu, L.; Laware, E.; Reckinger, N.; Didembourg, C.; Letesson, J.-J.; Sarrazin, M.; Deparis, O.; Matroule, J.-Y.; Colomer, J.-F. Do CVD Grown Graphene Films have Antibacterial Activity on Metallic Substrates? *Carbon* **2015**, *84*, 310−316.
(33) Li, J.; Wang, G.; Zhu, H.; Zhang, M.; Zheng, X.; Di, Z.; Liu, X.; Wang, X. Antibacterial Activity of Large-Area Monolayer Graphene Film Manipulated By Charge Transfer. *Sci. Rep.* **2014**, *4*, No. 4359.
(34) Hummers, W. S.; Offeman, R. E. Preparation of Graphitic Oxide. *J. Am. Chem. Soc.* **1958**, *80*, 1339.
(35) Marcano, D. C.; Kosynkin, D. V.; Berlin, J. M.; Sinitskii, A.; Sun, Z.; Slesarev, A.; Alemany, L. B.; Lu, W.; Tour, J. M. Improved Synthesis of Graphene Oxide. *ACS Nano* **2010**, *4*, 4806−4814.
(36) Dikin, D. A.; Stankovich, S.; Zimney, E. J.; Piner, R. D.; Dommett, G. H.; Evmenenko, G.; Nguyen, S. T.; Ruoff, R. S. Preparation and Characterization of Graphene Oxide Paper. *Nature* **2007**, *448*, 457−460.
(37) Putz, K. W.; Compton, O. C.; Segar, C.; Zhi, An; Nguyen, S. B. T.; Brinson, L. C. Evolution of Order during Vacuum-Assisted Self-Assembly of Graphene Oxide Paper and Associated Polymer Nanocomposites. *ACS Nano* **2011**, *5*, 6601−6609.
(38) Robinson, J. T.; Zalalutdinov, M.; Baldwin, J. W.; Snow, E. S.; Wei, Z.; Sheehan, P.; Houston, B. H. Wafer-Scale Reduced Graphene Oxide films for Nano Mechanical Devices. *Nano Lett.* **2008**, *8*, 3441−3445.
(39) Rodolfo, C.-S; Aaron, M.; Mauricio, T.; Ana, L. A.; Nestor, P.-L.; Morinobu, E. Method for Preparing Graphene Oxide Films and Fibers. U.S. Patent 9284193 B2, 2016.
(40) Paul, D. R. Creating New Types of Carbon-based Membranes. *Science* **2012**, *335*, 413−414.
(41) Rendueles, O.; Ghigo, J. M. Multi-species Biofilms: How to Avoid Unfriendly Neighbors. *FEMS Microbiol. Rev.* **2012**, *36*, 972−989.
(42) Silhavy, T. J.; Kahne, D.; Walker, S. The Bacterial Cell Envelope. *Cold Spring Harbor Perspect. Biol.* **2010**, *2*, No. a000414.
(43) Wang, L.; Hu, Chen.; Shao, L. The Antimicrobial Activity of Nanoparticles: Present Situation and Prospects for the Future. *Int. J. Nanomed.* **2017**, *12*, 1227−1249.
(44) Donlan, R. M. Biofilms: Microbial Life on Surfaces. *Emerging Infect. Dis.* **2002**, *8*, 881−890.
(45) Feng, G.; Cheng, Y.; Wang, S. Y.; Tascuic, D. A. B.; Worobo, R. W.; Moraru, C. I. Bacterial Attachment and Biofilm Formation on Surfaces are Reduced by Small-Diameter Nanoscale Pores: How Small is Small Enough? *npj Biofilms Microbiomes* **2015**, No. 15022.
(46) Sutherland, I. Biofilm Exopolysaccharides: A Strong and Sticky Framework. *Microbiology* **2001**, *147*, 3−9.
(47) Nel, A.; Xia, T.; Madler, L.; Li, N. Toxic Potential of Materials at the Nano Level. *Science* **2006**, *311*, 622−627.
(48) Lyon, D. Y.; Brunet, L.; Hinkal, G. W.; Wiesner, M. R.; Alvarez, P. J. J. Antibacterial Activity of Fullerene Water Suspensions (nC60) is not due to ROS-Mediated Damage. *Nano Lett.* **2008**, *8*, 1539−1543.
(49) Valko, M.; Morris, H.; Cronin, M. T. D. Metals, Toxicity and Oxidative Stress. *Curr. Med. Chem.* **2005**, *12*, 1161−1208.
(50) Nanda, S. S.; An, S. S. A.; Yi, D. K. Oxidative Stress and Antibacterial Properties of a Graphene Oxide-Cystamine Nanohybrid. *Int. J. Nanomed.* **2015**, *10*, 549−556.
(51) Becerra, M. C.; Albesa, I. Oxidative Stress Induced by Ciprofloxacin in *Staphylococcus aureus*. *Biochem. Biophys. Res. Commun.* **2002**, *297*, 1003−1007.
(52) O'Toole, G. A.; Kolter, R. Initiation of Biofilm Formation in *Pseudomonas fluorescens* WCS365 Proceeds via Multiple, Convergent Signaling Pathways: A Genetic Analysis. *Mol. Microbiol.* **1998**, *28*, 449−461.

DOI: 10.1021/acsomega.7b00371
ACS Omega 2017, 2, 3070−3082